MICROSCOPIC DESCRIPTION OF ^{252}Cf COLD FISSION YIELDS

M. MIREA[1], D.S. DELION[1,2], A. SĂNDULESCU[2,3]

[1]National Institute of Physics and Nuclear Engineering, 407 Atomiştilor, Bucharest-Măgurele, 077125 Romania
[2]Academy of Romanian Scientists, Splaiul Independenței 54, Bucharest, 050085 Romania
[3]Institute for Advanced Studies in Physics, Calea Victoriei 129, Bucharest, Romania

Received July 22, 2009

We investigate the cold fission of ^{252}Cf within the two center shell model to compute the potential energy surface. The fission yields are estimated by using the semiclassical penetration approach. It turns out that the inner cold valley of the total potential energy is strongly connected with Z=50 magic number. The agreement with experimental values is very much improved only by considering mass and charge asymmetry degrees of freedom. Thus, indeed cold fission of ^{252}Cf is a Sn-like radioactivity, related the other two "magic radioactivities", namely α-decay and heavycluster decay, called also Pb-like radioactivity. This calculation provides the necessary theoretical confidence to estimate the penetration cross section in producing superheavy nuclei, by using the inverse fusion process.

Key words: Cold fission, Superheavy nuclei, Potential surface, Cold valleys, Two center shell model, Woods-Saxon potential.

PACS numbers: 21.10.Dr, 21.10.Tg, 25.70.Jj, 25.85.Ca

I. INTRODUCTION

The synthesis of superheavy elements beyond Z = 104, suggested by Flerov [1], was predicted within the so-called fragmentation theory in Ref. [2] by using the cold valleys in the potential energy surface between different combinations, giving the same compound nucleus. Soon it was shown in Refs. [3, 4] that the most favorable combinations with $Z \geq 104$ are connected with the so-called Pb potential valley, i.e. the same valley of the heavy cluster emission [5].

Due to the double magicity of ^{48}Ca, similar with ^{208}Pb, in Ref. [4] it was proposed ^{48}Ca as a projectile on various transuranium targets. The production of many superheavy elements with $Z \leq 118$ (corresponding to the last stable element Cf) during last three decades was mainly based on this idea [6–9].

The shape of the potential energy versus various degrees of freedom plays an important role in predicting the fission/fusion probability to create superheavy nuclei. These processes take place along the so-called "cold valleys" of these surfaces. The

α-particle emission is connected with the "lightest" cold valley in the fragmentation potential surface. On the other hand the "heaviest" side of the cold valley is given by the cold fission process, i.e. the emission of two fragments with similar masses in their ground states. Between theses limits there is a broad region of cold heavy cluster decays. These decays are strongly connected with the ^{108}Pb-cold valley and this is the reason why they are also called "magic-radioactivities".

In order to check the validity of various approaches describing fission/fusion processes it is very important to reproduce experimentally measured yields. In this context we mention that systematic measurements were performed for ^{252}Cf [10, 11]. They correspond to various excitation energies of emitted fragments, including cold processes (neutronless), driven along the above mentioned cold valleys. The aim of this work is to describe the existing experimental cold fission data within a fully microscopic approach, namely the two-center shell model.

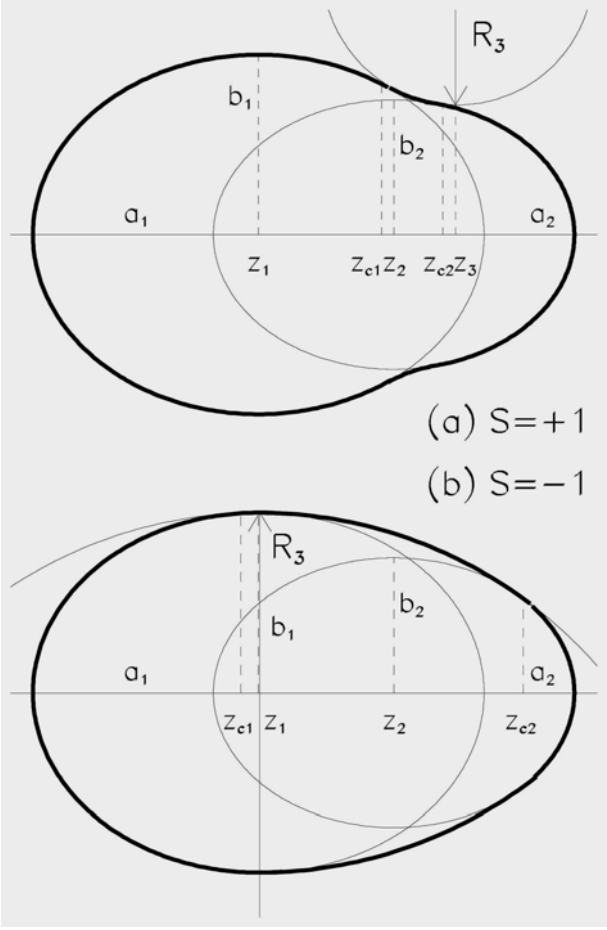

Fig. 1 – Nuclear shape parametrization.

In the past ^{252}Cf was investigated within the double folding potential method [12, 13] emphasizing the role of higher deformations in a correct description of the cold fission distribution of fragment yields. Therefore, the deformations introduced in our model take into account approximately the multipole deformations up to λ=4. In another work, based on a macroscopic model by determining the tip distances for the exit point from the barrier for ground state deformed fragments, it was predicted [14] that the major contribution in the yield distribution corresponds to the light fission fragment $A_2 \approx 100$.

II. THEORETICAL BACKGROUND

We extend the analysis performed in Ref. [15] within a simple model, to a more reliable microscopic approach to estimate the fission/fusion barrier, based on a new version of the Super Asymmetric Two Center Shell Model [16].

A nuclear shape parametrization, taking into account the relevant degrees of freedom encountered in fission, namely the elongation, the necking, the mass-asymmetry and the deformations of the fragments is used. In this context, shell corrections and cranking inertia are realistically determined. This model was already used in calculations of some superheavy elements [17].

The penetrability, corresponding to some binary partition, defines the isotopic yield and it is characterized by the difference between the nuclear plus Coulomb potential and the Q-value. For a given initial nucleus (Z, A) this quantity, called fragmentation potential, depends upon the charge, mass numbers of a given fragment (we will consider the second one) and the inter-fragment distance. For a fixed combination $A = A_1+A_2$ the fragmentation potential has a minimum at the charge equilibration point Z_2, which we will not mention in the following, i.e.

$$V(A_2, R) = V_N(A_2, R) + V_C(A_2, R) - Q, \tag{1}$$

where $V_N(A_2, R)$ is the nuclear and $V_C(A_2, R)$ Coulomb inter-fragment potential. We also introduced the Q-value in terms of the difference between binding energies of the parent and the sum of emitted fragments, i.e.

$$Q = B(Z, A) - B(Z_1, A_1) - B(Z_2, A_2). \tag{2}$$

For deformed nuclei, due to the fact that the largest emission probability corresponds to the lowest barrier, the deformation potential decreases in the direction of the largest fragment radius.

In most usual treatments of nuclear fission, the whole nuclear system is characterized by some collective coordinates associated to some degrees of freedom approximately determining the behavior of many intrinsic variables. The basic ingredient is the nuclear shape parametrization. The generalized coordinates vary in time, leading to the splitting of the nuclear system. In this work, the nuclear shape parametrization is obtained by smoothly joining two spheroids with a third

surface given by the rotation of a circle around the axis of symmetry. This parametrization is characterized by 5 degrees of freedom, namely the mass asymmetry, the elongation $R = z_2 - z_1$ given by the distance between the centers of the nascent fragments, the two deformations of the nascent fragments associated to the eccentricities $\varepsilon_i = \sqrt{1 - b_i^2 / a_i^2}$ (i=1,2), and the necking characterized by the curvature $C = S/R_3$ of the median surface and the mass-asymmetry term given by the ration of the semi-axis $\eta = a_1/a_2$. The notations used can be identified by inspecting the Fig. 1. Within this parametrization, swollen shapes in the median surface can be obtained for a negative curvature (S=–1) and necked ones for a positive curvature (S=1). The swollen configurations characterize the ground states, the shapes during the passage of the first barrier or the second well, while the necked configurations are associated to the passage of the second barrier.

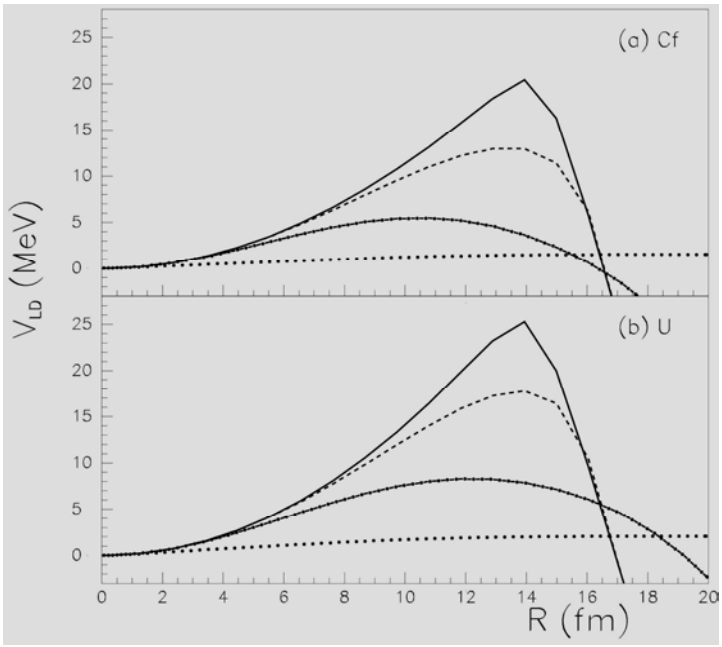

Fig. 2 – Liquid drop deformation energy as function of the elongation R for ^{252}Cf and ^{236}U as parents. Four values of the necking parameter are used. C=–0.1, 0.1, 0.5 and 100 fm^{-1} corresponding to the dotted, dash-dotted, dashed and full lines, respectively. In both cases, the light fragment is ^{95}Rb. The parent and the nascent fragments are considered spherical. The mass asymmetry is varied linearly from the initial sphere η=1 at R=0 fm to the final value at the touching configuration $R = r_0\left(A_1^{1/3} + A_2^{1/3}\right)$ (where r_0 is the reduced radius).

In order to estimate the fission yields it is necessary to investigate the penetration factor. This quantity can be estimated, as usually, by using the semiclassical integral [18]

$$P_{A_2} = \exp\left\{-2\int_{R_1}^{R_2}\sqrt{\frac{2\mu(A_2,R)}{\hbar^2}V(A_2,R)}dR\right\} \quad (3)$$

between internal and external turning points. Two ingredients are mandatory in order to evaluate the action integral: the fragmentation deformation energy V (we will call it simply deformation energy) and the inertial parameter μ.

In our calculation, the deformation energy of the nuclear system is the sum between the liquid drop energy V_{LD} and the shell effects δE, including pairing corrections [19], i.e.

$$V = V_{LD} + \delta E - V_0 \,. \quad (4)$$

The energy of the parent nucleus V_0 is used as a reference value, so that in the ground state configuration the deformation energy is zero and asymptotically, for two separated fragments at infinity, the deformation energy reaches the minus sum of energies of emitted fragments. Thus, the above Eq. (4) coincides with the definition given by Eq. (1).

The macroscopic energy is obtained within the framework of the Yukawa-plus-exponential model [20] extended for binary systems with different charge densities [21, 22]. The Strutinsky prescriptions [23] were computed on the basis of a new version of the superasymmetric two-center shell model. This version solves a Woods-Saxon potential in terms of the two-center prescriptions as detailed in Refs. [24, 25]. The inertial parameter μ is computed in the framework of the cranking model. In some particular evaluations, the values of the reduced mass is used. We considered only cold fission/fusion process. Consequently the deformations of the initial and final nuclei are given by their ground state values of Ref. [26].

III. NUMERICAL APPLICATION

For comparison with experimental data, the maximal values of the independent yields for a maximum excitation energy of 7 MeV were selected from Ref. [10]. The selected channels address binary partitions characterized by the following light fragments: ^{95}Rb, ^{96}Rb, ^{97}Sr, ^{98}Sr, ^{99}Y, ^{100}Y, ^{101}Zr, ^{102}Nb, ^{103}Zr, ^{104}Nb, ^{105}Mo, ^{106}Nb, ^{107}Mo, ^{108}Tc, ^{109}Mo, ^{110}Tc, ^{111}Ru, ^{112}Rh, ^{113}Ru, ^{114}Rh, ^{115}Rh, ^{116}Rh, ^{117}Pd, ^{118}Rh, ^{119}Pd, ^{120}Ag, ^{121}Cd and ^{122}Ag.

First of all, the fission trajectory in our five-dimensional configuration space must be supplied, that is a dependence between all generalized coordinates. This trajectory starts from the ground-state of the system and reaches the exit point of the barrier. The ground-state corresponds to the minimal deformation energy in the first well. In order to avoid a complicated determination of the minimal action trajectory, the deformations of the parent and those of the two fragments are taken from the literature [26]. A linear variation from initial values of the nascent fragments eccentricities and of the mass-asymmetry is postulated starting from the ground state

values of the parent up to the final ones, characterizing the fragments at the end of the fission process. The variation of the neck generalized coordinate was determined by using simple calculations of a minimal value of the liquid drop energy.

Dependencies of the liquid drop energy V_{LD} as a function of C and R are displayed in Fig. 2 for two nuclei, namely ^{236}U and ^{252}Cf. In these preliminary calculations, the deformations of the fragments are neglected. From the dependencies exhibited in these plots, it can be assessed that the influence of the neck parameter is crucial, the variations of V_{LD} exceeding several tens of MeV for small shifts of C. For Cf, up to R=17 fm the liquid drop deformation energy is always lower for negative values of C, that is for swollen shapes. For values of R >17 fm, the necked shapes are favored and the nucleus can be splitted into two separated fragments.

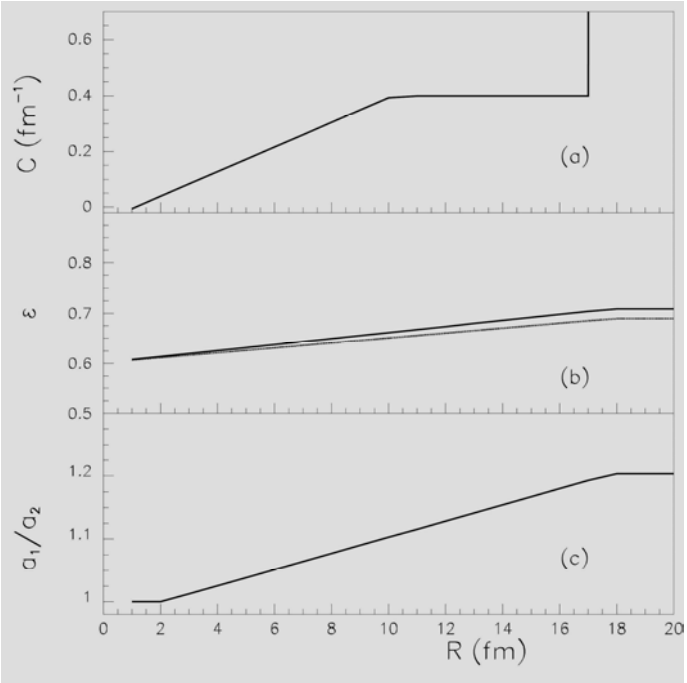

Fig. 3 – Variation of the generalized parameters as function of the elongation. (a) The necking parameter C varies linearly from the ground state configuration up to the region of the first barrier and remains constant up to the region of the second barrier. In the region of the second barrier the configurations are necked (that id C >0 fm^{-1}), and the neck vanishes at a value close to R= 17 fm. The deformations ε_1 and ε_2 of the fragments have a linear interpolation between the initial value of the parent up to the final values of the fragments at R=17 fm. A similar behavior is followed by the mass asymmetry parameter a_1/a_2.

From these simple considerations and by analyzing the macroscopic-microscopic energy in the case of ^{252}Cf for symmetric partitions, a particular

behavior of C as function of R was extracted. For very low values of the elongation, the values of C are considered negative, so the nucleus is swollen in the median part. Up to $R < 8$ fm, the curvature is varied linearly up to the value C=0.4 fm^{-1}. From R=8 fm up to the exit from the second barrier the neck is kept positive. The fact that the shapes are necked in the median surface implies the formation two individual fragments during the fission process itself, as expected in cold fission. Thus, at 17 fm, a sudden change of the curvature is postulated, so that, the shapes become very necked in the median region and the two nuclei are separated. The variations of the generalized coordinates as function of the elongation R are plotted in Fig. 3. Dependencies between the generalized coordinates q_i (i = 1, ...5) supply the fission trajectory. The shapes obtained within our nuclear shape parametrization are plotted in Fig. 4, starting from the ground state and reaching two separated deformed fragments.

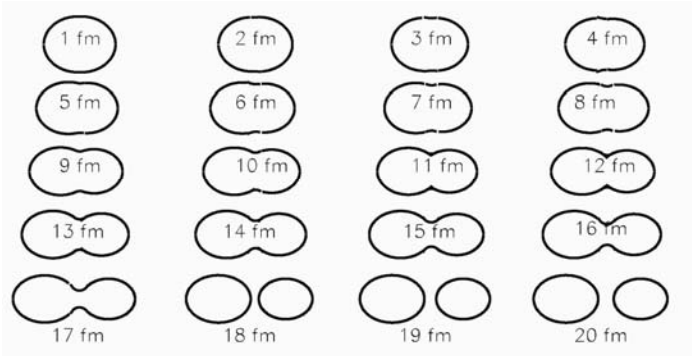

Fig. 4 – Family of nuclear shapes obtained along the fission path within the parametrization used in this work. The initial parent nucleus is ^{252}Cf and the light fragment is ^{95}Rb. The values of the elongation R are marked on the plot.

A complete description of the fission path requires the minimization of the action integral. Such calculations are very time consuming and they were performed up to now only for a single partition as in Refs. [27, 28]. In the actual calculations many channels have to be studied and such calculations are not feasible. To make our problem tractable, only one fission path is used for all investigated partitions.

By using the previous parametrization, the liquid drop deformation energy V_{LD} is computed for all selected binary partitions. The results are plotted in Fig. 5 as functions of the light fragment A_2 and the elongation R. It is interesting to notice that the liquid drop deformation energy exhibits a strong increase for the channels with A_2 >110. This variation is caused by the change of the ground state deformations of fission fragments, from prolate shapes to oblate ones. A first evalution is realized for transmissions of the liquid drop barrier.

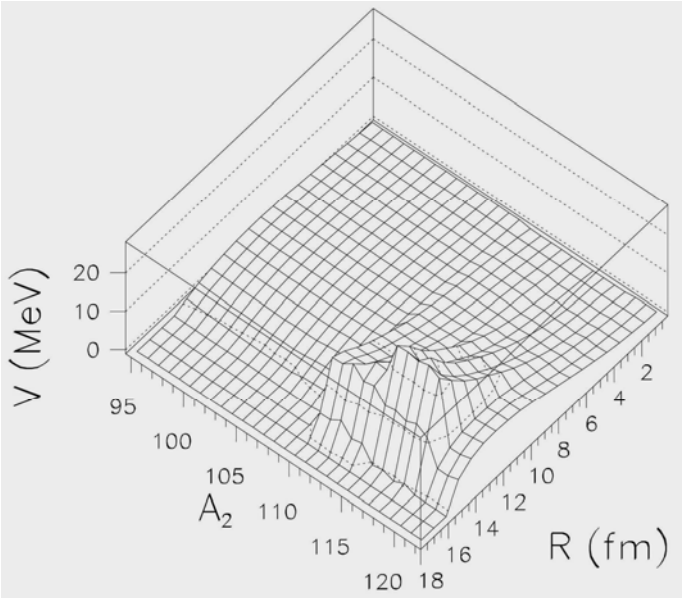

Fig. 5 – Lichid drop potential energy V_{LD} for the selected binary partitions with respect to A_2 and the elongation R.

The penetrabilities are computed using the WKB approximation by considering that the effective mass equals the reduced mass $\mu = \frac{A_1 A_2}{A}$ A of each partition. The theoretical penetrabilities, renormalized such that the maximal value is comparable to the maximum experimental yields, are plotted in Fig. 6. The maximal theoretical yield tends to be located around mass 103. The sudden drop of the penetrability at A_2=110 is due to a change in the deformations of the fragments. Up to A_2=110, both fission fragments are prolate while after A_2=110 the deformations become oblate. The liquid drop model fails to reproduce the experimental data. The maximum experimental yield is located at A_2=107 in the experimental data while the maximum theoretical transmission is given for A_2=104.

An improved description is expected by introducing shell and pairing effects in the framework of the microscopic-macroscopic model. By using the same fission paths, the deformation energy V is obtained in the framework of the microscopic-macroscopic model. The values of V are plotted in Fig. 7 as function of the elongation R and the light fragment mass A_2. Some general features of the fission barrier can be extracted. For A_2 <110 partitions, a double humped barrier is exhibited. An interesting feature can be observed in the region of the second well, where a global minimum for A_2=110 and $R \approx 8$ fm (the starting point of two arrows in the lower panel of Fig. 7) is clearly evidenced. This minimum indicates a possible isomeric state. In Fig. 8, two barriers corresponding to two different partitions with A_2=100 and 110 are plotted.

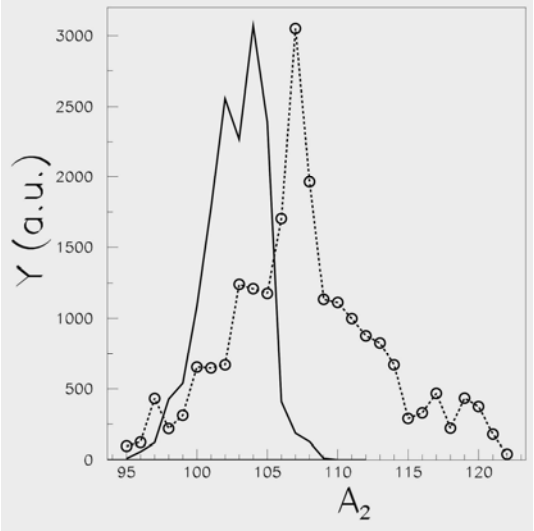

Fig. 6 – Experimental yields in arbitrary units (dashed line), compared with renormalized theoretical penetrabilities calculated within the liquid drop model (solid line) with respect to A_2.

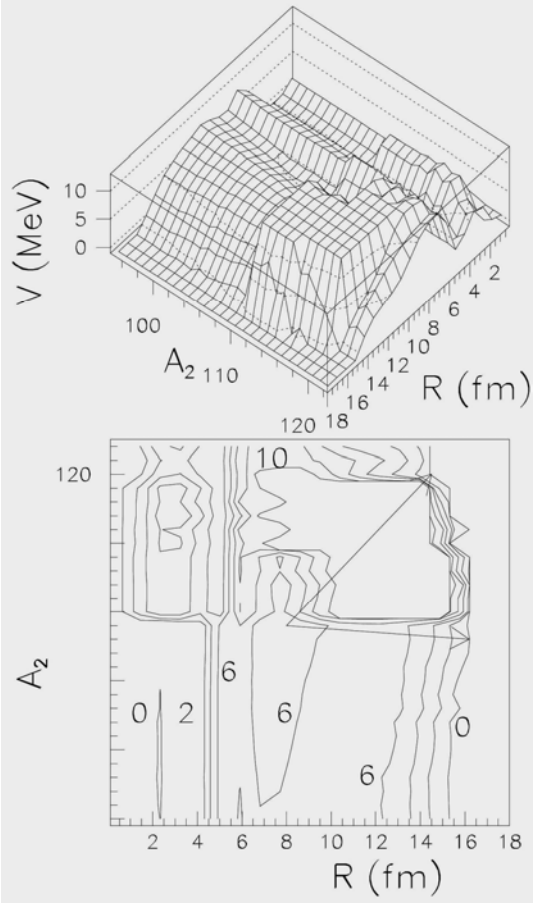

Fig. 7 – Deformation energy V computed within the microscopic-macroscopic method for different binary partitions with respect to A_2 and the elongation R. In the lower plot, the equipotential contours are plotted in step of 2 MeV. Some values of the deformation energy are marked.

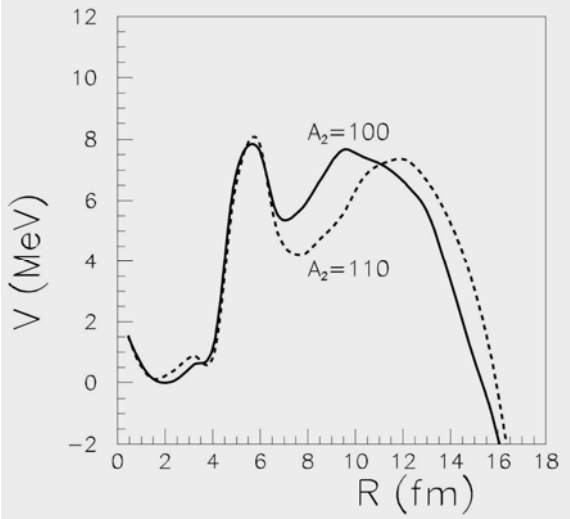

Fig. 8 – Fission barriers obtained for two different partitions as function of the elongation. The mass of the light fragment is marked on the plot.

In both cases, the inner barriers have comparable values and shapes, but the second minimum is lowered for higher A_2. On the other hand, the shapes of the external barriers are changed dramatically when the mass-asymmetry varies. The external barrier is lower for A_2=110 than for A_2=100. In the same time, the external barrier is thinner for A_2=100. The competition of these two effects are canceling when the transmission is computed. In order to evaluate the influence of the deformation energy on the fragment yields, the action integral has to be evaluated. In this context, the inertia is computed within the cranking approximation [29] within the formula

$$\begin{aligned}\mu = B_{RR} + B_{CC}\left(\frac{\partial C}{\partial R}\right)^2 + B_{\eta\eta}\left(\frac{\partial \eta}{\partial R}\right)^2 + B_{\varepsilon_1\varepsilon_1}\left(\frac{\partial \varepsilon_1}{\partial R}\right)^2 + B_{\varepsilon_2\varepsilon_2}\left(\frac{\partial \varepsilon_2}{\partial R}\right)^2 + \\ + 2B_{C\eta}\frac{\partial C}{\partial R}\frac{\partial \eta}{\partial R} + 2B_{C\varepsilon_1}\frac{\partial C}{\partial R}\frac{\partial \varepsilon_1}{\partial R} + 2B_{C\varepsilon_2}\frac{\partial C}{\partial R}\frac{\partial \varepsilon_2}{\partial R} + \\ + 2B_{\eta\varepsilon_1}\frac{\partial \eta}{\partial R}\frac{\partial \varepsilon_1}{\partial R} + 2B_{\eta\varepsilon_2}\frac{\partial \eta}{\partial R}\frac{\partial \varepsilon_2}{\partial R} + 2B_{\varepsilon_1\varepsilon_2}\frac{\partial \varepsilon_1}{\partial R}\frac{\partial \varepsilon_2}{\partial R},\end{aligned} \tag{5}$$

where B_{ij} are the elements of the effective mass tensor. The resulting effective mass along the postulated trajectory is plotted on Fig. 9. For comparison with experimental data, the theoretical yields are considered proportional with the transmission.

The penetrabilities of the fission barrier, obtained in the frame of the microscopic-macroscopic model for zero excitation energy, are displayed in Fig. 10. These penetrabilities reflect the interplay between the values of the deformation energy and the inertia along a given fission path. Unfortunately, the theoretical transmissions are not able to reproduce the main trends observed in the experimental distribution of fission yields. By introducing the shell effects, our results are even worse that those obtained within the simple liquid drop framework.

Two peaks in the theoretical penetrabilities are observed at A_2=97 and 120, while the maximum experimental yield is located at A_2=107.

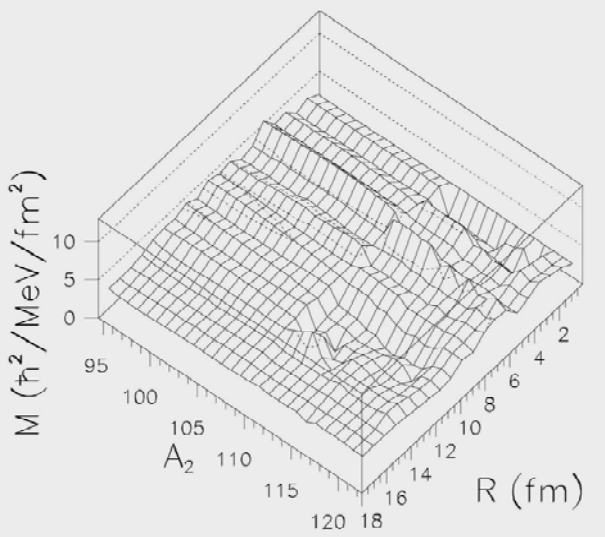

Fig. 9 – Effective mass computed within the cranking approximation for different binary partitions with respect to A_2 and the elongation R.

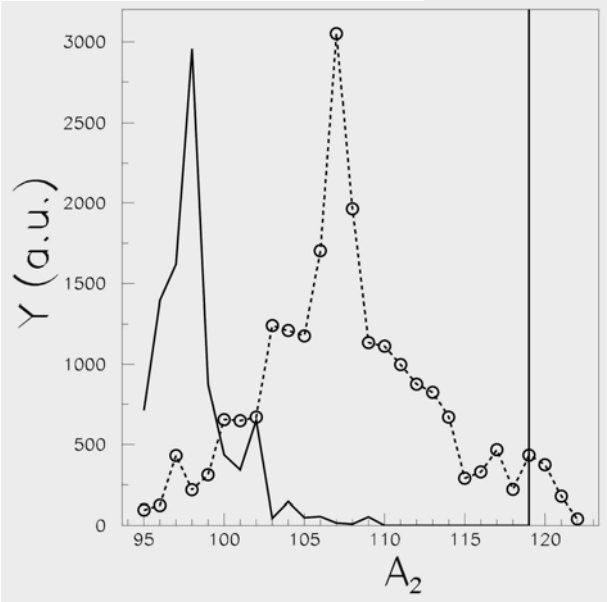

Fig. 10 – Experimental yields in arbitrary units (dashed line), compared with renormalized theoretical penetrabilities calculated within the microscopic-macroscopic model (solid line) with respect to A_2.

Thus, a direct transmission of the barrier is not consistent with experimental data. Therefore another effect should describe the yields distribution, this effect being neglected in our calculations. It is worth mentioning that similar results are obtained in Fig. 11 by using the double folding procedure [13], by using the same deformation parameters and neglecting the mass asymmetry.

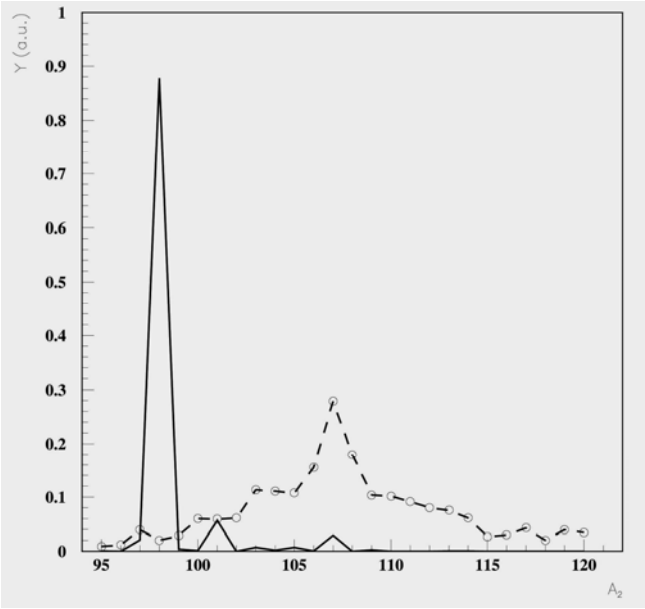

Fig. 11 – Experimental yields in arbitrary units (dashed line), compared with renormalized theoretical penetrabilities calculated within the double folding model (solid line) with respect to A_2.

It is possible that the cold fission follows another fission path that takes into consideration the existence of a global minimum in the second well, that is the cold fission trajectory must proceed through the isomer configuration. In these circumstances we consider that the penetrability must be produced in two steps: first of all the isomeric state in the second well is reached and afterwards, the second barrier is penetrated. As previously mentioned, the isomeric state is located at A_2=110 and $R \approx 8$ fm. From this isomeric state, the nuclear shapes and mass asymmetry are modified linearly such that at the exit point of the barrier, the final shapes of the fragments are reached as displayed by the arrows plotted on the lower panel of Fig. 7. The isomer minimum is considered axial symmetric.

The microscopic-macroscopic deformation energy starting only from the isomeric state up to the formation of two separated fragments is plotted in Fig. 12. The generalized shape coordinates change linearly from the isomeric configuration values to the final ones at the exit point of the external barrier. The inertia computed in the framework of the cranking model is displayed in Fig. 13. With these ingredients, the calculated penetrabilities at zero excitation energies through the external barrier are compared with experimental yields on Fig. 14. In this last approximation it is implicitly assumed that the penetration of the inner barrier is the same for all partitions, so that differences in the barrier transmission between channels are managed only by the external barrier.

A very good agreement between the theoretical penetrability distribution and the experimental yields is obtained for $A_2 < 110$. The maximum theoretical value is obtained at A_2=106 while the maximum experimental yield is found at A_2=107. A sudden drop of theoretical penetrabilities is theoretically obtained for channels

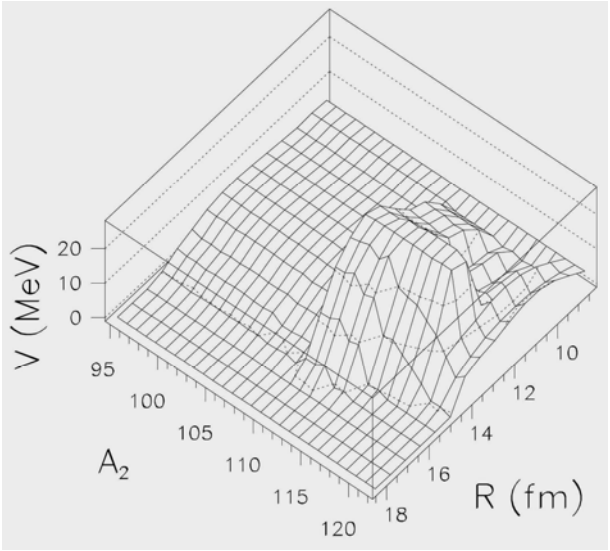

Fig. 12 – Deformation energy V calculated within the microscopic-macroscopic method for different binary partitions with respect to A_2 and the elongation R beginning from the minimum energy configuration of the second well and varying linearly all generalized coordinates up to the scission point.

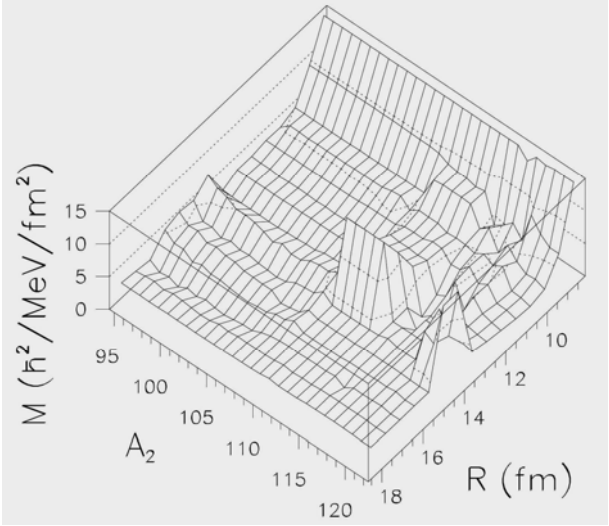

Fig. 13 – Effective mass computed in the cranking approximation for different binary partitions with respect to A_2 and the elongation R in the region of the second barrier.

characterized by $A_2 > 110$. As previously noticed, this behavior is connected with the ground state shapes of fragments that become oblate for these channels. Perhaps these oblate shapes are not the best configurations during the penetration of the barrier, and the final ground state oblate configurations are obtained only after the exit from the fission barrier. It is important to notice that, in order to reproduce the experimental data, a crucial hypothesis was made, namely the cold fission is considered intimately connected to the deformations of the ground state of nascent fragments. In general, the fission process is more favorable for prolate nuclear

shapes and it is possible that our hypothesis is no longer valid. Therefore, it can be expected that the fission process proceed through prolate deformations of the fragments and the oblate ground state shapes are obtained only after the exit from the outer barrier. An enhancement of the fission probability is obtained for A_2=120. I must be noticed that experimentally, a special situation is encountered in cold fission of ^{252}Cf with one fragment being the ^{132}Sn [30, 31]. Here the yield shows an enhancement for very exciation energies. Such a structure was observed only for fragmentations close to ^{132}Sn. There is an indication that can be a cluster mode fission. This enhancement was also reproduced by our calculations.

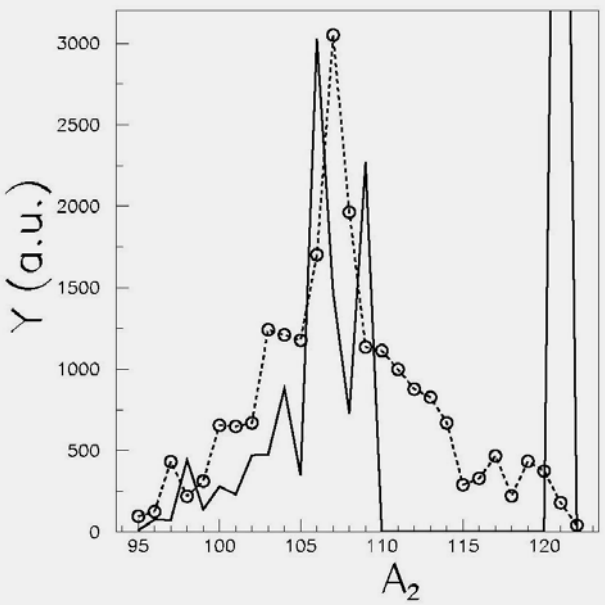

Fig. 14 – Experimental yields in arbitrary units (dashed line), compared with renormalized theoretical penetrabilities calculated within the microscopic-macroscopic model (solid line) with respect to A_2 by taking into account the minimum energy in the second well.

IV. CONCLUSIONS

Concluding, we computed the potential energy surface for different binary combinations, giving the superheavy compound nucleus $^{252}_{98}$Cf by using the Two Center Shell Model. We obtained a satisfactory agreement of the experimental yields by considering variable mass and charge asymmetry beyond the first barrier of the potential surface. The cold fission is strongly connected with Z=50 magic number, because an enhancement of the fission probability was obtained for $^{120}_{47}$Ag+$^{132}_{51}$Sb partition. The low value of the deformation energy in the isomeric microscopic configuration reflects the magicity of the Sn proton number. It was evidenced that a good agreement with experimental data can be obtained only if the fission path proceeds through this isomeric configuration. The final transmissions

are managed only by the external barrier, showing a strong dependence on the final fragment shapes. Due to the fact that prolate shapes are more favorable for the fission process, the maximal values of the yields are shifted towards channels characterized by lower values of A_2. Thus, the cold fission process of ^{252}Cf can be called Tin-like radioactivity, similar with with the Led-like radioactivity, corresponding to various heavy cluster emission processes.

Acknowledgements. This work was supported by the contract IDEI-119 of the Romanian Ministry of Education and Research.

REFERRENCES

1. G.N. Flerov, Atom. Ener. **26,** 138 (1969).
2. A. Săndulescu, R.K. Gupta, W. Scheid, and W. Greiner, Phys. Lett. **60** B, 225 (1976).
3. R.K. Gupta, C. Parvulescu, A. Săandulescu, and W. Greiner, Z. Phys. A **283,** 217 (1977).
4. R.K. Gupta, A. Săndulescu, and W. Greiner, Phys. Lett. **67** B, 257 (1977).
5. A. Săndulescu, D. Poenaru, and W. Greiner, Fiz. Elem. Chastits At. Yadra 11, 1334; Sov. J. Part. Nucl. **11,** 528 (1980).
6. Yu. Ts. Oganessian, Nucl. Phys. A **685**, 17c (2001).
7. Yu. Ts. Oganessian, *et. al.,* Nucl. Phys. A **734,** 109 (2004).
8. S. Hofmann and G. Münzenberg, Rev. Mod. Phys. **72,** 733 (2000).
9. S. Hofmann, G. Münzenberg, and M. Schädel, Nucl. Phys. News 14 No. 4, 5 (2004).
10. F.-J. Hambsch, H.-H. Knitter, and C. Budtz-Jorgensen, Nucl. Phys. A **554**, 209 (1993).
11. H.-H. Knitter, F.-J. Hambsch, and C. Budtz-Jorgensen, Nucl. Phys. A **536**, 221 (1992).
12. A. Săndulescu, A. Florescu, F. Carstoiu, W. Greiner, J.H. Hamilton, A.V. Ramayya, and B.R.S. Babu, Phys. Rev. C **54**, 258 (1996).
13. A. Săndulescu, Ş. Mişicu, F. Carstoiu, A. Florescu, and W. Greiner, Phys. Rev. C **57**, 2321 (1998).
14. F. Gonnenwein, and B. Borsig, Nucl. Phys. A **530**, 27 (1991).
15. D.S. Delion and A. Săndulescu, Rom. J. Phys. **52**, 43 (2007).
16. M. Mirea, Phys. Rev. C **57**, 2484 (1998).
17. M. Mirea, D.S. Delion, and A. Sandulescu, EPL **85**, 12001 (2009).
18. G. Gamow Z. Phys. **51**, 204 (1928).
19. J.R. Nix, Ann. Rev. of Nucl. Sci. **22**, 65 (1972).
20. K.T.R. Davies, and J.R. Nix, Phys. Rev. C **14**, 1977 (1976).
21. D.N. Poenaru, M. Ivascu, and D. Mazilu, Comput. Phys. Commun. **19**, 205 (1980).
22. M. Mirea, O. Bajeat, F. Clapier, F. Ibrahim, A.C. Mueller, N. Pauwels, and J. Proust, Eur. Phys. J. A **11**, 59 (2001).
23. M. Brack, J. Damgaard, A. Jensen, H. Pauli, V. Strutinsky, and W. Wong, Rev. Mod. Phys. **44,** 320 (1972).
24. M. Mirea, Rom. Rep. Phys. **59**, 523 (2007).
25. M. Mirea, Phys. Rev. C **78,** 044618 (2008).
26. P. Möller, J.R. Nix, W.D. Myers, and W.J. Swyatecki, At. Data Nucl. Data Tables **59**, 185 (1995).
27. M. Mirea, L. Tassan-got, C. Stephan, C.O. Bacri, R.C. Bobulescu, Phys.Rev. C **76**, 064608 (2007).
28. M. Mirea, and L. Tassan-Got, Rom. J. Phys., **54**, 331 (2009).
29. M. Mirea, R.C. Bobulescu, and M. Petre, Rom. Rep. Phys., **61**, 646 (2009).
30. F. Gonnenwein, Proc. Int. Conf. on Fission and Properties of Neutron-Rich Nuclei, Sanibel Island, Florida (Nov. 1997).
31. H.-G. Clerc, in Heavy Elements and Related New Phenomena, Eds. W. Greiner and R.K. Gupta, World Scientific, p. 451 (1999).